Chinese Journal of Chemical Engineering, **20**(1) 111—119 (2012)

Process Characteristics of CO_2 Absorption by Aqueous Monoethanolamine in a Microchannel Reactor*

YE Chunbo (叶春波)[1,2], **CHEN Guangwen** (陈光文)[1,**] **and YUAN Quan** (袁权)[1]
[1] Dalian Institute of Chemical Physics, Chinese Academy of Sciences, Dalian 116023, China
[2] Graduate School, Chinese Academy of Sciences, Beijing 100049, China

Abstract Process characteristics of CO_2 absorption using aqueous monoethanolamine (MEA) in a microchannel reactor were investigated experimentally in this work. A T-type rectangular microchannel with a hydraulic diameter of 408 μm was used. Operating parameters, *i.e*. temperature, pressure and molar ratio of MEA to CO_2 were studied. Under 3 MPa pressure, the mole fraction of CO_2 in gas phase could decrease from 32.3% to 300×10^{-6} at least when gas hourly space velocity ranged from 14400 to 68600 h^{-1} and molar ratio of MEA to CO_2 was kept at 2.2. In particular, the effects of temperature on CO_2 absorption flux, mass transfer driving force, gas-liquid contact time and enhancement factor were analyzed in detail and found that mass transfer enhancement by chemical reaction was a crucial factor for the process of CO_2 absorption.
Keywords miniaturization, microchannel, microfluidic, carbon dioxide, absorption, monoethanolamine

1 INTRODUCTION

Carbon dioxide (CO_2), as a greenhouse gas, is the main contributor to the observed global warming [1]. Therefore, it is of great importance to remove large amounts of CO_2 from natural, refinery and synthesis gas streams. Many different options are available for this purpose, but the most widely utilized technique is the absorption by alkanolamine-based chemical solvents, such as monoethanolamine (MEA) [2–4], diethanolamine (DEA) [5], mixed amines of piperazine (PZ) and methyldiethanolamine (MDEA) [6, 7], *etc*.

Aqueous MEA, as an important absorbent in the CO_2 removal process, has many advantages, such as high reactivity, low solvent cost, low molecular mass and thus high absorption capacity on a mass basis, reasonable thermal stability, *etc* [8]. Sometimes it can be used as an activator and mix with other amines [9, 10]. Recently, MEA solutions have received much attention in the area of CO_2 capture and storage.

As an important parameter, CO_2 solubility in MEA solutions has been measured at temperatures from 0 to 150 °C and pressures from 0.5 Pa to 20 MPa in a stirred cell reactor with long equilibrium time [11–13]. When temperature increases or pressure decreases, the solubility reduces as expected. Besides, a number of mathematical models, such as Deshmukh-Mather model [14] and Kent-Eisenberg model [15], are also developed to predict CO_2 solubility in alkanolamine systems. The concentration of each ion in CO_2-MEA system can be obtained from the modeling results.

With respect to the reaction kinetics between CO_2 and MEA solutions, however, discrepancies always exist in the published data on reaction rate constants, as reviewed in Ref. [16]. When determining the reaction rate constants in a laminar jet absorber [17], a stirred cell reactor [18], or a wetted wall column [9], the experimental data could be explained with an assumption of pseudo-first order reaction regime, due to the limited mass transfer capacities of these equipments and the absence of interfacial turbulence. However, when the absorption was carried out at short contact time [19], the reaction between CO_2 and MEA could be considered to be practically instantaneous.

Up to now, the process of CO_2 absorption into MEA solutions has been investigated extensively. Kim *et al*. [20] predicted the enthalpy of CO_2 absorption into MEA solutions from equilibrium constants and pointed out that the enthalpy decreased with CO_2 loading. Akanksha and Srivastave [2] reported the gas side mass transfer coefficient for the case of countercurrent gas-liquid flow in a falling film microreactor and observed that mass transfer rate strongly depended on gas and liquid flow rates. Maceiras and Alvarez [21] investigated the effect of temperature on the volumetric mass transfer coefficient in a bubble column. The volumetric mass transfer coefficient was deduced depending on the two film theory and an assumption of instantaneous reaction regime between CO_2 and MEA. Freguia and Rochelle [4] analyzed the sensitivity of process variables in a system consisting of a packed absorber, a stripper and a cross heat exchanger, with the aim to find operating conditions at low energy consumption based on a RateFrac absorber model.

Current absorption processes usually involve absorption towers and packed or plate columns [22–25], which have huge volumes and relatively low efficiencies in mass transfer. Hence, there is a need to develop new technologies that can miniaturize reaction and unit operation elements and integrate these process devices in order to save space and energy.

Received 2010-05-18, accepted 2010-11-10.
* Supported by the National Natural Science Foundation of China (20911130358), the Ministry of Science and Technology of China (2009CB219903), and the Fund of Dalian Institute of Chemical Physics, CAS (K2009D01).
** To whom correspondence should be addressed. E-mail: gwchen@dicp.ac.cn

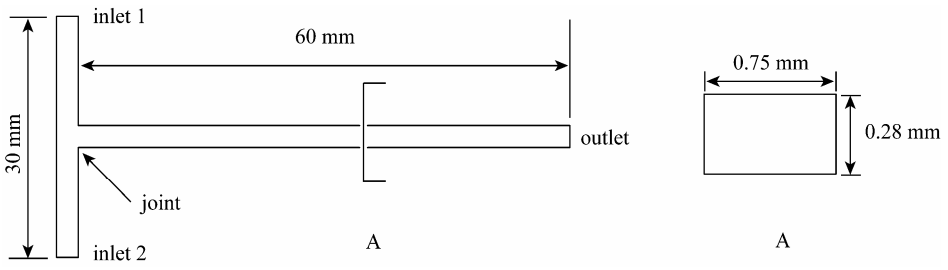

(1) Top view (2) Cross-section of the microchannel

Figure 1 Specific dimensions of the microchannel used in the CO_2 absorption process

Microchannel, as a novel tool for process intensification, is well-known for its merits, such as excellent mass and heat transfer abilities, huge surface to volume ratio, short diffusion distance, narrow residence time distribution, small volume, *etc*., and shows great potential in the processes of gas absorption [26], hydrogenation [27], nitration [28], extraction [29] and so on.

In this paper, process characteristics of CO_2 absorption into aqueous MEA were first time investigated in a microchannel reactor. The influences of operating parameters, *i.e*. temperature, pressure and molar ratio of MEA to CO_2, on the process of CO_2 absorption were investigated. In particular, the effects of temperature, one of the most important parameters, on CO_2 absorption flux, mass transfer driving force, gas-liquid contact time and enhancement factor were elucidated in detail in order to get a fundamental understanding of the process.

2 EXPERIMENTAL

2.1 Materials

Feed gas, a mixture of CO_2 and nitrogen (N_2), was utilized. MEA with a purity of 99.5%, provided by Tianjin Guangfu Fine Chemical Research Institute, was used without further purification, while deionized water was boiled in order to remove the dissolved gases before utilization. MEA solution with a mass fraction of 30% was prepared from the MEA and the boiled deionized water by mass.

2.2 Specific dimensions of the microchannel

Specific dimensions of the T-type, rectangular microchannel utilized in this work are shown in Fig. 1, including the top and the cross-section view. The distance between inlets 1 and 2 is 30 mm, while the distance from the joint to the outlet is 60 mm. The joint is at the middle place between inlets 1 and 2. The width and the depth equal to 0.75 mm and 0.28 mm, respectively. The microchannel was fabricated on a 316L stainless steel plate by micromachining technology, with another stainless steel plate as cover plate. The two plates were bonded *via* vacuum diffusion bonding.

Based on the above information, the hydraulic diameter (D_h) of the channel and the specific surface area (a_s) of the channel from the joint to the outlet are 0.408 mm and 9809.5 $m^2 \cdot m^{-3}$, respectively, which are calculated from the following equations:

$$D_h = 2wd/(w+d) \quad (1)$$

$$a_s = 2(w+d)L/(wdL) \quad (2)$$

where w and d denote the width and the depth of the microchannel, respectively, and L is the length of the channel from the joint to the outlet.

2.3 Experimental setup and methodology

The schematic of the experimental setup for CO_2 absorption process is shown in Fig. 2, mainly consisted of a home-made microchannel reactor, a gas-liquid separator, a mass flow controller, a constant-flow pump, a gas cylinder and a test section. The test section contains a soap film flowmeter and a CO_2 sensor.

The temperature of the microchannel reactor was governed by a waterbath with an accuracy of ±0.1 K. Two coiled stainless steel tubes with an inner diameter of 2 mm and a thickness of 0.5 mm placed in water bath were connected with inlets 1 and 2, respectively. When the gas and liquid flowed through the tubes, the given temperature could be attained. The inlet and the outlet pressure were measured by two pressure transducers, and the pressure drop of the main channel from the joint to the outlet was estimated by a differential pressure transducer (Huba Control AG, 692), respectively. The feed gas was regulated by a mass flow controller (Beijing Sevenstar Electronics Company, measurement range: 0−10 $L \cdot min^{-1}$), while MEA solution was transferred by a constant-flow pump (Scientific Systems Inc, measurement range: 0−10 $ml \cdot min^{-1}$) to contact the feed gas at the joint of microchannel. After flowing through the microchannel, the gas-liquid two phases were separated immediately *via* the gas-liquid separator, where CO_2 absorption was small enough and could be neglected according to a blank experiment. The length, inner diameter and thickness of the stainless steel tube connecting the microchannel reactor and the separator was 35 mm, 4 mm and 1 mm, respectively. After separation, the liquid

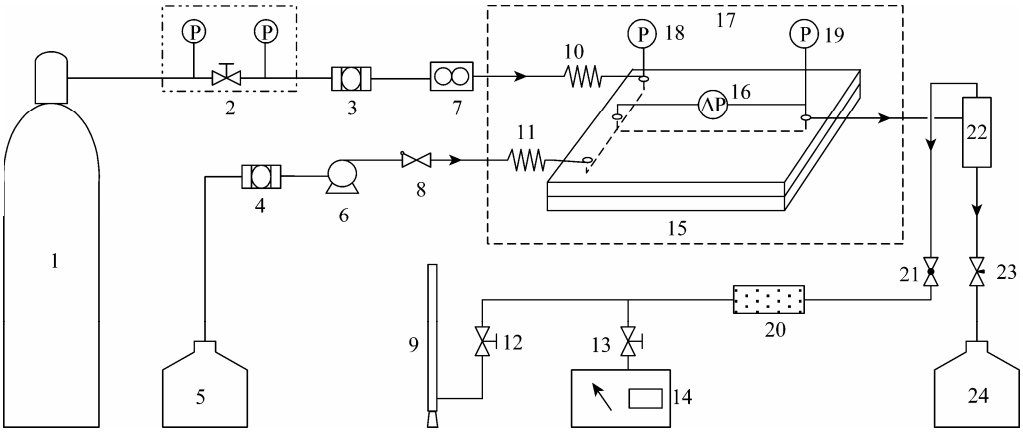

Figure 2 Schematic of the experimental setup for the CO_2 absorption process
1—gas cylinder; 2—pressure reducing valve; 3, 4—filter; 5—fresh solution tank; 6—constant-flow pump; 7—mass flow controller; 8—check valve; 9—soap film flowmeter; 10, 11—coil; 12, 13—adjusting valve; 14—CO_2 sensor; 15—microchannel reactor; 16—differential pressure transducer; 17—thermostatic waterbath; 18, 19—pressure transducer; 20—silica gel drier; 21—back pressure valve; 22—gas-liquid separator; 23—needle valve; 24—rich solution tank

directly flowed into the rich solution tank, while the gas flowed through a silica gel drier to remove trace amounts of MEA solution. The drier had been swept by the feed gas for an hour before conducting CO_2 absorption experiments. The concentration of CO_2 was analyzed by a CO_2 sensor with detection limit of 300×10^{-6} (Ennix Inc, FG10), and the flow rate was determined by the soap film flowmeter. When CO_2 concentration did not changed within 2 min, its value was recorded. All experiments have been repeated for two times at least, the relative deviation did not exceed 1%.

CO_2 conversion, X, which was based on the difference between CO_2 molar flow rates at the inlet and the outlet, was used to evaluate the performance of microchannel in CO_2 absorption process:

$$X = \left(n_{CO_2,in} - n_{CO_2,out}\right)\Big/ n_{CO_2,in} \times 100\% \quad (3)$$

where n denotes the molar flow rate.

When calculating CO_2 conversion, the solubility of N_2 in MEA solution was assumed to be neglected. In order to examine this assumption, the error of N_2 molar flow rates between the inlet and the outlet of microchannel was calculated as

$$E_{N_2} = \left(n_{N_2,in} - n_{N_2,out}\right)\Big/ n_{N_2,in} \times 100\% \quad (4)$$

In this work, the value of E_{N_2} was less than 2%. The molar flow rate of N_2, n_{N_2}, was determined based on the volumetric flow rate and the concentration of CO_2 of gas phase.

For convenience and comparison, the feed gas flow rate, determined by the soap film flowmeter at 25 °C at the inlet of microchannel, was used to calculate gas hourly space velocity (GHSV):

$$U_G = \frac{Q_{G,in}}{wdL}\frac{P_0}{P} \quad (5)$$

where $Q_{G,in}$ is the volumetric flow rate of feed gas at 25 °C at the inlet, $m^3\cdot h^{-1}$. P_0 is ambient pressure, 0.1 MPa. When CO_2 absorption was conducted at high pressure P, P_0/P was used to modify the calculation of U_G.

When analyzing the two-phase flow pattern, the superficial velocities of gas and liquid phases were applied and estimated with

$$j_G = Q_{G,in}/(3600wd) \quad (6)$$

$$j_L = Q_{L,in}/(3600wd) \quad (7)$$

where j denotes the superficial velocity, $m\cdot s^{-1}$. The volumetric flow rate of gas at 25 °C and the liquid flow rate at the inlet were used directly to calculate the superficial velocities.

3 THEORY

3.1 Reaction mechanism

Aqueous MEA solution is an important absorbent in the CO_2 capture process due to its nature as primary amine. When CO_2 reacts with MEA, the carbamate formation reaction occurs:

$$CO_2 + 2MEA \rightleftharpoons MEACOO^- + MEAH^+ \quad (8)$$

which is considered to be practically instantaneous [19, 21]. Besides, high temperature is beneficial to the reversibility of this reaction [30], and thus can make the absorption rate slower and hinder the process of CO_2 absorption [31, 32].

According to the zwitterion mechanism which is widely justified [4, 20, 21], the reaction steps usually involve the formation of a zwitterion,

$$CO_2 + MEA \rightleftharpoons MEAH^+COO^- \quad (9)$$

and the subsequent deprotonation of the zwitterion by a base B,

$$MEAH^+COO^- + B \rightleftharpoons MEACOO^- + BH^+ \quad (10)$$

where B is a base that can be MEA, OH^-, CO_3^{2-}, HCO_3^- or H_2O. In this work, CO_2 loading is never more than 0.5 mol of CO_2 per mol of MEA after absorption. Under this condition, the main products in the rich solution are $MEAH^+$ and $MEACOO^-$, while the concentrations of OH^-, CO_3^{2-}, HCO_3^-, and especially the free CO_2 are very low [16]. Therefore, the deprotonation of the zwitterion comes mainly from MEA, and to a less extent, from OH^-, CO_3^{2-}, HCO_3^- or H_2O, since the deprotonation ability of a base depends mainly on its concentration and basicity [33].

3.2 Physical properties

Density and dynamic viscosity of MEA solution were estimated from the work of Amundsen *et al*. [34] and Weiland *et al* [35]. The influences of MEA concentration, CO_2 loading and temperature on density and viscosity were all taken into account in their experiments.

According to Henry's law, the gas-liquid equilibrium can be achieved at the gas-liquid interface and the relationship can be described as follows:

$$P_{CO_2} = HC_{CO_2,i} \tag{11}$$

where $C_{CO_2,i}$ is the CO_2 concentration at the interface, $mol\cdot L^{-1}$. Henry's constant, $kPa\cdot L\cdot mol^{-1}$, was determined with Eq. (12) proposed by Versteeg and Swaaij [36],

$$H = 2.8429\times10^6 \exp(-2044/T) \tag{12}$$

The diffusion coefficient of CO_2 in MEA solution was estimated by N_2O analogy. The diffusion coefficients of CO_2 and N_2O in water were calculated using the following equations [36, 37], respectively,

$$D_{CO_2,H_2O} = 2.35\times10^{-6} \exp(-2119/T) \tag{13}$$

$$D_{N_2O,H_2O} = 5.07\times10^{-6} \exp(-2371/T) \tag{14}$$

The diffusion coefficient of N_2O into aqueous MEA solution was calculated using [36]

$$D_{N_2O}\mu_{MEA}^{\gamma} = D_{N_2O,H_2O}\mu_{H_2O}^{\gamma} \tag{15}$$

where γ was equal to 0.51 in MEA solution [38]. The dynamics viscosity of water was obtained from the work by Korson *et al* [39].

Then the diffusion coefficient of CO_2 in MEA solution could be calculated using the N_2O analogy:

$$\frac{D_{CO_2}}{D_{N_2O}} = \frac{D_{CO_2,H_2O}}{D_{N_2O,H_2O}} \tag{16}$$

The diffusivity coefficient of MEA in water was estimated from the equation proposed by Maceiras and Alvarez [21],

$$D_{MEA} = 3.586\times10^{-15} T/\mu_{MEA} \tag{17}$$

3.3 Absorption rate model

CO_2 absorption flux, N_{CO_2}, is calculated by the following equation:

$$N_{CO_2} = \left(n_{CO_2,in} - n_{CO_2,out}\right)/(aV) = k_L^* \Delta C_{CO_2,m} \tag{18}$$

where a is the interfacial area per volume, and V is the volume of the main microchannel from the joint to the outlet.

From the work of Yue *et al*. [40], when the ratio of the volumetric flow rates of gas to liquid exceeds 50 and the gas superficial velocity is more than 10 $m\cdot s^{-1}$, the interfacial area is approximately equal to the specific surface area of the microchannel, because under this condition, gas-liquid two phase flow is in annular flow or churn flow regime and the thickness of the liquid film is very thin. So we have

$$aV = 2(w+d)L \tag{19}$$

In the experiments, CO_2 loading, molar ratio of absorbed CO_2 to MEA in the rich solution, was never more than 0.5. Therefore, the concentration of free CO_2 in the liquid bulk could be assumed to be zero. The logarithmic mean values of CO_2 concentration in the interface between the inlet and the outlet could be used as the approximation of the mass transfer driving force:

$$\begin{aligned}\Delta C_{CO_2,in} &= \frac{C_{CO_2,i,in} - C_{CO_2,i,out}}{\ln\left(C_{CO_2,i,in}/C_{CO_2,i,out}\right)} \\ &= \frac{1}{H}\frac{P_{CO_2,in} - P_{CO_2,out}}{\ln\left(P_{CO_2,in}/P_{CO_2,out}\right)}\end{aligned} \tag{20}$$

Then the liquid-phase mass transfer coefficient for chemical absorption of CO_2, k_L^*, could be deduced from Eqs. (18)–(20).

The liquid-phase mass transfer coefficient for physical absorption of CO_2 was defined as Eq. (21) based on Higbie's penetration model [41]. The values obtained by Eq. 21 at 25 °C were approximate to those estimated by the correlation for CO_2 physical absorption under the slug-annular flow and the annular flow in microchannel at 20 °C [40],

$$k_L = 2\sqrt{\frac{D_{CO_2}}{\pi\tau}} \tag{21}$$

When calculating gas-liquid contact time (τ), it is necessary to modify the flow rate of gas according to the experimental conditions, for temperature, pressure and CO_2 concentration all have influences on the gas volumetric flow rate. In this work, the gas phase could be treated as ideal gas [42]. The flow rate is modified by

$$Q_{avg} = \left(Q_{in} + Q_{out}\right)/2 \tag{22}$$

$$Q_G = Q_{avg}\left(P_0 / P\right)\left(T / T_0\right) \quad (23)$$

where T_0 is the reference temperature, 298.15 K.

The contact time is calculated by

$$\tau = 3600wdL/\left(Q_G + Q_L\right) \quad (24)$$

The enhancement factor of CO_2 absorption, E, which is a measure of the effect of chemical reaction on mass transfer, can be determined using

$$E = k_L^* / k_L \quad (25)$$

for free CO_2 in the bulk solution can be considered to be zero [41].

4 RESULTS AND DISCUSSION

4.1 Absorption results at 3 MPa pressure

The results of CO_2 absorption in the microchannel reactor under 3 MPa pressure were demonstrated in Fig. 3. The concentration of CO_2 in feed gas was 32.3% (by volume) and U_G was in the range from 1.44×10^4 to 6.86×10^4 h^{-1}. When the molar ratio of MEA to CO_2 was kept at 2.2, the conversion of CO_2, at least, attained to 99.94% at 25 or 45 °C. Even the molar ratio of MEA to CO_2 was reduced to 2 which equaled the stoichiometric ratio, the conversion of CO_2 was still higher than 91% at 25 °C. The two peak values in Fig. 3 (a) may be closely related to the flow characteristics of gas-liquid two-phase flow in the microchannel, since the superficial velocities of gas and liquid rose together with the increase in U_G. Further research was needed to confirm this conception.

When U_G increased from 1.19×10^5 to 2.08×10^5 h^{-1}, as shown in Fig. 3 (b), CO_2 conversion was still very high. At 2.2 molar ratio of MEA to CO_2, the minimum of the conversion was 92.7%, while when the molar ratio was equal to 2, the conversion decreased slightly, and the minimum was 88.4%.

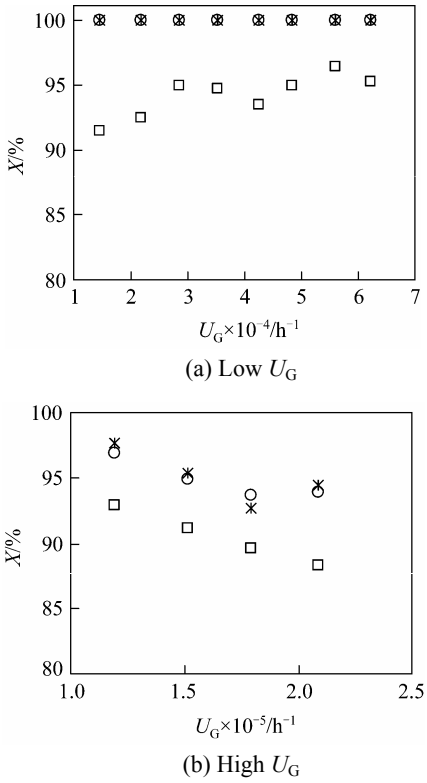

Figure 3 Results of CO_2 absorption at 3 MPa pressure
✳ 25 °C, 2.2 [MEA/CO_2 (by mol)]; □ 25 °C, 2.0 [MEA/CO_2 (by mol)]; ○ 45 °C, 2.2 [MEA/CO_2 (by mol)]

4.2 Absorption results at ambient pressure

When investigating the process of CO_2 absorption at ambient pressure, the molar ratio of MEA to CO_2 was kept constant at 2.2 and the concentration of CO_2 in feed gas was 29.8% by volume.

Compared Fig. 4 (a) with Fig. 3 (a), CO_2 conversions at ambient pressure were lower than those obtained at 3 MPa. The conversions at 25, 45 and 65 °C all decreased as UG increased and varied from 91% to 80%, but the tendency brought about by temperature was not obvious.

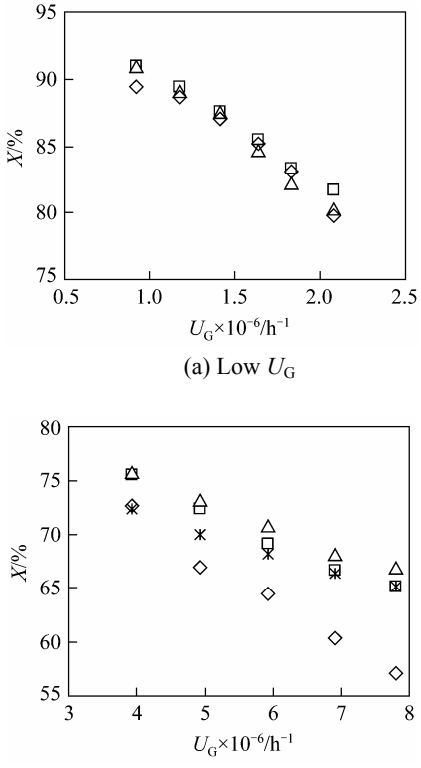

Figure 4 Results of CO_2 absorption at ambient pressure and 2.2 MEA/CO_2 (by mol)
temperature/°C: ◇ 25; □ 45; △ 65; ✳ 85

At higher U_G ranging from 3.93×10^6 to 7.80×10^6 h^{-1}, as displayed in Fig. 4 (b), CO_2 conversion was in

the range from 76% to 57%, which decreased gradually as GHSV increased. What's more, it increased when temperature was raised from 25 to 65 °C. However, when temperature reached 85 °C, CO_2 conversion was smaller than that at 45 °C. Compared with Fig. 4 (a), the gas-liquid contact time was reduced due to the increase of U_G, which was the main reason for the apparent tendency of CO_2 conversions at 25, 45 and 65 °C in Fig. 4 (b). Because that at higher GHSV, mass transfer by convection would be improved, but a higher U_G would result in a shorter contact time and hence less consumption of CO_2 by reaction.

From above results, we can see that high pressure is beneficial to the process of CO_2 absorption, because the equilibrium solubility of CO_2 in aqueous MEA solution increased with pressure [11, 43] and the gas-liquid contact time can be prolonged greatly at high pressure, due to the compressibility of the gas phase. Besides, higher molar ratio of MEA to CO_2 is also favorable for CO_2 absorption, for that at higher molar ratio, more MEA can react with CO_2, which will lead to a faster absorption rate for CO_2 capture.

4.3 Influences of temperature on CO_2 absorption

As shown in Fig. 4 (b), the effects of temperature on CO_2 absorption are obvious at ambient pressure and high U_G and will be elucidated in this section, since diffusion coefficients of CO_2 and MEA in solution, Henry's constant, gas-liquid contact time and reaction rate constant are all temperature dependent.

4.3.1 *Flow pattern analysis*

Some researchers have investigated the gas-liquid two-phase flow patterns in microchannel, and found that two-phase flow pattern primarily depended on superficial velocities of gas and liquid phases. In addition, two-phase flow pattern maps in microchannel were similar with each other, although microchannels with different hydraulic diameters and different gas and liquid phases were applied [40, 44–46].

Kawahara *et al*. [44] investigated experimentally the gas-liquid two-phase flow in a 100 μm diameter circular tube. Deionized water and N_2 were utilized as gas and liquid phases, respectively. From the flow regime maps provided, we could see that the two-phase flow was probable in annular flow regime or churn flow regime when the gas superficial velocity exceeded 20 $m \cdot s^{-1}$ and the liquid superficial velocity varied from 0 to 1 $m \cdot s^{-1}$. Similar results could be found in the work of Yue *et al*. [40], who investigated the two-phase flow patterns of water-CO_2 in a rectangular microchannel with a hydraulic diameter of 667 μm.

In this work, the hydraulic diameter of the T-type rectangular microchannel was 408 μm. The superficial velocity of the liquid phase varied from 0.356 to 0.707 $m \cdot s^{-1}$, while the superficial velocity of gas phase exceeded 50 $m \cdot s^{-1}$, depending on the flow rates at the inlet of microchannel. Under these conditions, the two-phase flow was in the range of annular flow or churn flow regime.

4.3.2 *Influences of temperature*

Based on the above flow pattern analysis, CO_2 absorption flux was determined using Eq. (18). In Fig. 4 (b) the ratio of the volumetric flow rates of gas to liquid almost approached 180 and the gas superficial velocity exceeded 50 $m \cdot s^{-1}$. Under such condition, it was feasible to replace the interfacial area with the specific surface area of the microchannel. As presented in Fig. 5, CO_2 absorption flux varied from 0.98 to 1.80 $mol \cdot m^{-2} \cdot s^{-1}$, and ascended with U_G. Because more gas and liquid would flow through the microchannel as U_G increased. CO_2 absorption flux in this work was at least one order of magnitude higher than that in a falling film microreactor [47].

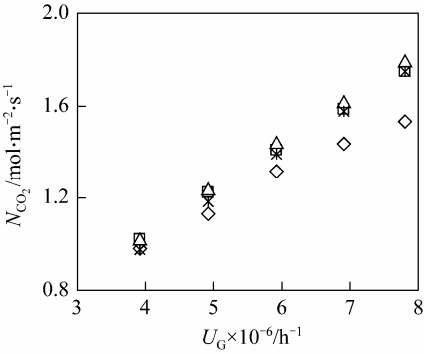

Figure 5 Effects of temperature on CO_2 absorption flux at ambient pressure and 2.2 MEA/CO_2 (by mol)
temperature/°C: ◇25; □45; △65; ✳85

As shown in Fig. 6, the mass transfer driving force decreased as temperature went up from 25 to 85 °C. It was mainly attributed to the reduction of CO_2 solubility in MEA solution [11], which could hinder the process of CO_2 transferring from gas to liquid.

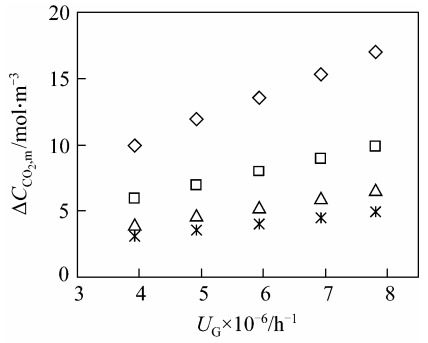

Figure 6 Effects of temperature on mass transfer driving force at ambient pressure and 2.2 MEA/CO_2 (by mol)
temperature/°C: ◇25; □45; △65; ✳85

As revealed in Fig. 7, the liquid side mass transfer coefficient went up with temperature obviously. As temperature increased, the diffusion coefficients of CO_2 and MEA increased, and the viscosity of MEA

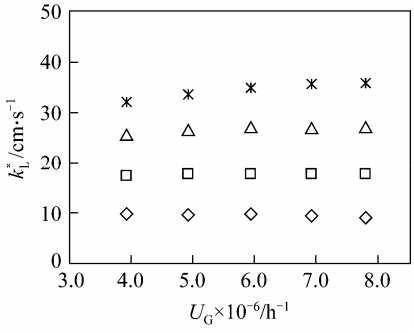

Figure 7 Effects of temperature on liquid side mass transfer coefficient at ambient pressure and 2.2 MEA/CO_2 (by mol)
temperature/°C: ◇25; □45; △65; ✳85

solution would decreased, which were favorable for the mass transfer process. The reaction between CO_2 and MEA would also be enhanced as temperature increased, and thus resulted in larger enhancement factors, which was demonstrated in Fig. 8. Due to the mass transfer enhancement by chemical reaction, the liquid side mass transfer coefficient was in the range from 0.09 to 0.358 m·s^{-1}, which was one or two orders of magnitude higher than that in the physical absorption of CO_2 in microchannel [40].

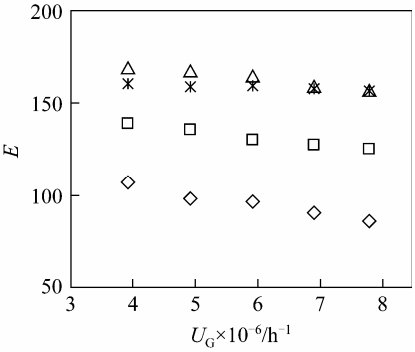

Figure 8 Effects of temperature on enhancement factor at ambient pressure and 2.2 MEA/CO_2 (by mol)
temperature/°C: ◇25; □45; △65; ✳85

In addition, the liquid side mass transfer coefficient was hardly influenced by U_G at the temperatures from 25 to 65 °C, but at 85 °C, the coefficient slightly went up with U_G. At higher temperatures, the mass transfer enhancement by reaction was offset by the desorption process of CO_2 from MEA solution [30] and the mass transfer resistance would become significant. The increase of the liquid side mass transfer coefficient with U_G at 85 °C was mainly due to the reduction of mass transfer resistance with U_G.

As demonstrated in Fig. 8, when the temperature increased from 25 to 65 °C, the reaction rate must increase according to Arrhenius Equation, and besides, the diffusion coefficient of CO_2 would ascend from 1.1×10^{-9} to 2.4×10^{-9} m^2·s^{-1}, and D_{MEA} from 3.8×10^{-10} to 8.2×10^{-10} m^2·s^{-1}, while the liquid viscosity decreased from 2.8 to 1.5 mPa·s. These aspects enhanced the absorption process effectively, which could overcome the negative influences of the decrease in CO_2 solubility and the gas-liquid contact time. Besides, the enhancement factor at 85 °C was less than that at 65 °C. The reason may be that CO_2 desorption from MEA solution was more obvious, and thus reduced the absorption rate at 85 °C [30]. The tendency of enhancement factor with temperature revealed the importance of chemical reaction in the process of CO_2 absorption in Fig. 4 (b).

As displayed in Fig. 9, the contact time varied from 0.99 to 1.62 ms and decreased with temperature and U_G simultaneously. At the same U_G, the contact time decreased with temperature gradually due to the expansibility of gas phase. Compared with Fig. 4 (b), the tendency of contact time with temperature was contrary to the trend of CO_2 conversion with temperature from 25 to 65 °C, which could be mainly attributed to the mass transfer enhancement by chemical reaction.

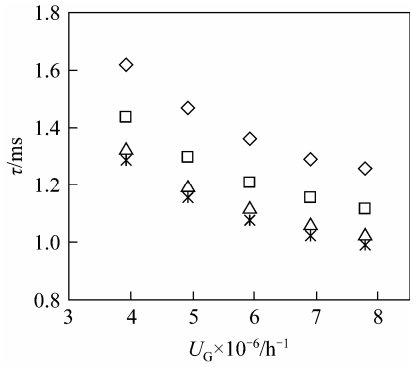

Figure 9 Effects of temperature on the gas-liquid contact time at ambient pressure and 2.2 MEA/CO_2 (by mol)
temperature/°C: ◇25; □45; △65; ✳85

From above analysis, we could see that mass transfer enhancement by chemical reaction was a crucial factor in the process of CO_2 absorption into aqueous MEA solution in the microchannel reactor. As temperature increased, although the mass transfer driving force and gas-liquid contact time decreased obviously, the mass transfer coefficient with reaction ascended gradually which was mainly due to the chemical enhancement. On the other hand, the tendency of enhancement factor with temperature also revealed the importance of chemical reaction.

5 CONCLUSIONS

Microchannel showed excellent performance in CO_2 absorption process. At 3 MPa pressure, CO_2 absorption could reach 99.94% at least when U_G was in the range of 1.44×10^4 and 6.86×10^4 h^{-1}, and molar ratio of MEA to CO_2 was kept at 2.2. Under ambient pressure and lower molar ratio of MEA to CO_2, the capacity of microchannel in CO_2 absorption process would be weakened slightly.

With respect to the influence of temperature on CO_2 absorption at ambient pressure, the tendencies brought about by temperature on CO_2 absorption flux, mass transfer driving force, gas-liquid contact time and enhancement factor were presented and discussed, and found that mass transfer enhancement by chemical reaction was the major contributor to the excellent performance of microchannel in the process of CO_2 absorption.

Process characteristics of CO_2 absorption in the work reveal that microchannel reactor is one of the most potential equipments for CO_2 absorption and can enhance the process efficiency greatly. Compared with absorption towers and packed or plate columns, microreactor can reduce the reactor volume and eliminate flooding at high flow rates, and hence, shows promising prospect for the CO_2 absorption process.

NOMENCLATURE

a	interfacial area, $m^2 \cdot m^{-3}$
a_s	specific surface area, $m^2 \cdot m^{-3}$
B	base
C	concentration, $mol \cdot L^{-1}$
$\Delta C_{CO_2,m}$	logarithmic mean values of CO_2 concentrations, $mol \cdot m^{-3}$
D	diffusion coefficient in MEA solution, $m^2 \cdot s^{-1}$
D_h	hydraulic diameter, m
d	depth, m
E	enhancement factor
E_{N_2}	error in N_2 molar flow rates between the inlet and the outlet of microchannel
H	Henry's law constant, $kPa \cdot L \cdot mol^{-1}$
j	superficial velocity, $m \cdot s^{-1}$
k_L	liquid mass transfer coefficient for physical absorption, $cm \cdot s^{-1}$
k_L^*	liquid mass transfer coefficient for chemical absorption, $cm \cdot s^{-1}$
L	length of microchannel from the joint to the outlet, m
N	absorption flux, $mol \cdot m^{-2} \cdot s^{-1}$
n	molar flow rate, $mol \cdot s^{-1}$
P	pressure, kPa
Q	volumetric flow rate, $m^3 \cdot h^{-1}$
T	temperature, K
U_G	gas hourly space velocity, h^{-1}
w	width, m
X	CO_2 conversion
μ	dynamic viscosity, Pa·s
τ	gas liquid contact time, s

Superscripts

γ	index number for MEA

Subscripts

avg	average
G	gas
i	interface
in	inlet
L	liquid
out	outlet

REFERENCES

1 Bernard, T., "Primary energy sources and greenhouse effect", *C. R. Geosci*., **335** (6-7), 597−601 (2003).

2 Akanksha, K.P., Srivastava, V., "Mass transport correlation for CO_2 absorption in aqueous monoethanolamine in a continuous film contactor", *Chem. Eng. Process*., **47** (5), 920−928 (2008).

3 Akanksha, K.P., Srivastava, V., "Carbon dioxide absorption into monoethanolamine in a continuous film contactor", *Chem. Eng. J*., **133** (1-3), 229−237 (2007).

4 Freguia, S., Rochelle, T.G., "Modeling of CO_2 capture by aqueous monoethanolamine", *AIChE. J*., **49** (7), 1676−1686 (2003).

5 Hikita, H., Asai, S., Ishikawa, H., Uku, K., "Absorption of carbon-dioxide into aqueous diethanolamine solutions", *Chem. Eng. Commun*., **5** (5-6), 315−322 (1980).

6 Xu, G.W., Zhang, C.F., Qin, S.J., Zheng, Z.S., "A kinetics study on the absorption of carbon dioxide into a mixed aqueous solution of methyldiethanolamine and piperazine", *Ind. Eng. Chem. Res*., **40**, 3785−3791 (2001).

7 Bishnoi, S., Rochelle, G.T., "Absorption of carbon dioxide in aqueous piperazine / methyldiethanolamine", *AIChE. J*., **48** (12), 2788−2799 (2002).

8 McCann, N., Maeder, M., Attalla, M., "Simulation of enthalpy and capacity of CO_2 absorption by aqueous amine systems", *Ind. Eng. Chem. Res*., **47** (6), 2002−2009 (2008).

9 Xiao, J., Li, C.W., Li, M.H., "Kinetics of absorption of carbon dioxide into aqueous solutions of 2-amino-2-methyl- 1-propanol plus monoethanolamine", *Chem. Eng. Sci*., **55** (1), 161−175 (2000).

10 Mandal, B.P., Bandyopadhyay, S.S., "Absorption of carbon dioxide into aqueous blends of 2-amino-2-methyl- 1-propanol and monoethanolamine", *Chem. Eng. Sci*., **61** (16), 5440−5447 (2006).

11 Jou, F.Y., Mather, A.E., Otto, F.D., "The solubility of CO_2 in a 30-mass-percent monoethanolamine solution", *Can. J. Chem. Eng*., **73** (1), 140−147 (1995).

12 Ma' mun, S., Nilsen, R., Svendsen, H.F., "Solubility of carbon dioxide in 30 mass % monoethanolamine and 50 mass % methyldiethanolamine", *J. Chem. Eng. Data*. **50** (2), 630−634 (2005).

13 Shen, K.P., Li, M.H., "Solubility of carbon dioxide in aqueous mixtures of monoethanolamine with methyldiethanol- amine", *J. Chem. Eng. Data*, **37** (1), 96−100 (1992).

14 Deshmukh, R.D., Mather, A.E., "A mathematical model for equilibrium solubility of hydrogen sulfide and carbon dioxide in aqueous alkanolamine solutions", *Chem. Eng. Sci*., **36**, 355−362 (1981).

15 Kent, R.L., Elsenberg, B., "Better data for amine treating", *Hydrocarbon. Process*., **55**, 87−90 (1976).

16 Aboudheir, A., "Kinetics of the reactive absorption of carbon dioxide in high CO_2-loaded, concentrated aqueous monoeth- anolamine solutions", *Chem. Eng. Sci*., **58** (23-24), 5195−5210 (2003).

17 Sada, E., Kumazawa, H., Butt, M.A., Hayashi, D., "Simultaneous absorption of carbon dioxide and hydrogen sulfide into aqueous monoethanolamine solutions", *Chem. Eng. Sci*., **31** (9), 839−841 (1976).

18 Sada, E., Kumazawa, H., Han, Z.Q., "Chemical absorption of carbon dioxide into ethanolamine solutions of polar solvent", *AIChE. J*., **32** (2), 347−349 (1986).

19 Clarke, J.K.A., "Kinetics of absorption of carbon dioxide in monoethanolamine solutions at short contact times", *Ind. Eng. Chem. Res*., **3** (3), 239−245 (1964).

20 Kim, I., Karl, A.H., Erik, T.H., Warberg, T.H., Svendsen, H.F., "Enthalpy of absorption of CO_2 with alkanolamine solutions predicted from reaction equilibrium constants", *Chem. Eng. Sci*., **64** (9), 2027−2038 (2009).

21 Maceiras, R.E., Álvarez, M.Á.C., "Effect of temperature on carbon dioxide absorption in monoethanolamine solutions", *Chem. Eng. J*., **138** (1-3), 295−300 (2008).

22 Fair, J.R., Seibert, A.F., Behrens, M., Saraber, P.P., Olujic, Z., "Structured packing performance-experimental evaluation of two predictive models", *Ind. Eng. Chem. Res*., **39** (6), 1788−1796 (2000).

23 Krumdieck, S., Wallace, J., Curnow, O., "Compact, low energy CO_2 management using amine solution in a packed bubble column", *Chem. Eng. J*., **135** (1-2), 3−9 (2008).

24 Sundaresan, A., Varma, Y.B.G., "Interfacial area and mass transfer in gas-liquid cocurrent upflow and countercurrent flow in reciprocating plate column", *Can. J. Chem. Eng*., **68** (6), 952−958 (1990).

25 Faramarzi, L., Kontogeorgis, G.M., Michelsen, M.L., Thomsen, K., Stenby, E.H., "Absorber model for CO_2 capture by monoethanolamine", *Ind. Eng. Chem. Res*., **49** (8), 3751−3759 (2010).

26 Chen, G.W., Yue, J., Quan, Q., "Gas-liquid microreaction technology: recent developments and future challenges", *Chin. J. Chem. Eng.*, **16** (5), 663−669 (2008).

27 Kobayashi, J., Mori, Y., Kobayashi, S., "Hydrogenation reactions using scCO(2) as a solvent in microchannel reactors", *Chem. Commun.*, (20), 2567−2568 (2005).

28 Shen, J.N., Zhao, Y.C., Chen, G.W., Yuan, Q., "Investigation of nitration processes of iso-octanol with mixed acid in a microreactor", *Chin. J. Chem. Eng.*, **17** (3), 412−418 (2009).

29 Su, Y.H., Chen, G.W., Zhao, Y.C., Yuan, Q., "Intensification of liquid-liquid two-phase mass transfer by gas agitation in a microchannel", *AIChE. J.*, **55** (8), 1948−1958 (2009).

30 Jamal, A., Meisen, A., Lim, C.J., "Kinetics of carbon dioxide absorption and desorption in aqueous alkanolamine solutions using a novel hemispherical contactor (I) Experimental apparatus and mathematical modeling", *Chem. Eng. Sci.*, **61** (19), 6571−6589 (2006).

31 Jamal, A., Meisen, A., Lim, C.J., "Kinetics of carbon dioxide absorption and desorption in aqueous alkanolamine solutions using a novel hemispherical contactor (I) Experimental results and parameter estimation", *Chem. Eng. Sci.*, **61** (19), 6590−6603 (2006).

32 Versteeg, G.F., Laj, V.D., van Swaaij, W.P.M., "On the kinetics between CO_2 and alkanolamines both in aqueous and non-aqueous solutions. An overview", *Chem. Eng. Commun.*, **144**, 113−158 (1996).

33 Mandal, B.P., Biswas, A.K., Bandyopadhyay, S.S., "Absorption of carbon dioxide into aqueous blends of 2-amino-2-methyl-1-propanol and diethanolamine", *Chem. Eng. Sci.*, **58** (18), 4137−4144 (2003).

34 Amundsen, T.G., Oi, L.E., Eimer, D.A., "Density and viscosity of monoethanolamine plus water plus carbon dioxide from (25 to 80) °C", *J. Chem. Eng. Data*, **54**, 3096−3100 (2009).

35 Weiland, R.H., Dingman, J.C., Cronin, D.B., Browning, G.J., "Density and viscosity of some partially carbonated aqueous alkanolamine solutions and their blends", *J. Chem. Eng. Data*, **43**, 378−382 (1998).

36 Versteeg, G.F., van Swaaij, W.P.M., "Solubility and diffusivity of acid gases(CO_2, N_2O) in aqueous alkanolamine solutions", *J. Chem. Eng. Data*, **33**, 29−34 (1988).

37 Versteeg, G.F., Blauwhoff, P., van Swaaij, W.P.M., "The effect of diffusivity on gas-liquid mass transfer in stirred vessels. Experiments at atmospheric and elevated pressures", *Chem. Eng. Sci.*, **42**, 1103−1109 (1987).

38 Sada, E., Kumazawa, H., Butt, M.A., "Solubility and diffusivity of gases in aqueous solutions of amines", *J. Chem. Eng. Data*, **23**, 161−163 (1978).

39 Korson, L., Drosthan, W., Millero, F.J., "Viscosity of water at various temperatures", *J. Phys. Chem.*, **73** (1), 34−39 (1969).

40 Yue, J., Chen, G.W., Yuan, Q., Luo, L., Gonthier, Y., "Hydrodynamics and mass transfer characteristics in gas-liquid flow through a rectangular microchannel", *Chem. Eng. Sci.*, **62** (7), 2096−2108 (2007).

41 Danckwerts, P.V., Gas Liquid Reactions, McGraw-Hill, New York (1970).

42 Span, R., Lemmon, E.W., Jacobsen, R.T., Wagner, W., Yokozeki, A., "A reference equation of state for the thermodynamic properties of nitrogen for temperatures from 63.151 to 1000 K and pressures to 2200 MPa", *J. Phys. Chem. Ref. Data*, **29** (6), 1361−1433 (2000).

43 Mathonat, C., Majer, V., Mather, A.E., Grolier, J.P.E., "Use of flow calorimetry for determining enthalpies of absorption and the solubility of CO_2 in aqueous monoethanolamine solutions", *Ind. Eng. Chem. Res.*, **37** (10), 4136−4141 (1998).

44 Kawahara, A., Chung, P.M.Y., Kawaji, M., "Investigation of two-phase flow pattern, void fraction and pressure drop in a microchannel", *Int. J. Multiphase. Flow*, **28**, 1411−1435 (2002).

45 Triplett, K.A., Ghiaasiaan, S.M., Abdel-Khalik, S.I., Sadowski, D.L., "Gas-liquid two-phase flow in microchannels - Part I: two-phase flow patterns", *Int. J. Multiphase. Flow*, **25** (3), 377−394 (1999).

46 Zhao, T.S., Bi, Q.C., "Co-current air-water two-phase flow patterns in vertical triangular microchannels", *Int. J. Multiphase. Flow.*, **27** (5), 765−782 (2001).

47 Sobieszuk, P., Pohorecki, R., "Gas-side mass transfer coefficients in a falling film microreactor", *Chem. Eng. Process.*, **49** (8), 820−824 (2010).